Nanostructures

DOI: 10.1002/ange.200804630

Formation of Hierarchical InAs Nanoring/GaAs Nanowire Heterostructures**

Mohanchand Paladugu, Jin Zou, Ya-Nan Guo, Xin Zhang, Hannah J. Joyce, Qiang Gao, H. Hoe Tan, Chennupati Jagadish,* and Yong Kim*

Materials in low dimensions exhibit unique properties,[1] and they are scientifically important for the realization of the fundamentals of self-assembly of matter.[2] Semiconductor quantum wells (two-dimensional) and quantum dots (zero-dimensional) are both examples of such low-dimensional systems, which have made a significant contribution to the development of global technology.[1] Nanowires, on the other hand, are ideal candidates to explore the growth and physical properties of materials in one dimension.[3,4] Semiconductor nanowires exhibit properties that are potentially useful for a wide variety of applications, including nanoelectronic and nano-optoelectronic devices and biosensors.[5] Fabrication of axial and radial nanowire heterostructures, including branched and hierarchical heterostructures, has further broadened the potential applications of these nanostructures.[4,6,7] Nanowire heterostructures are generally grown by the vapor–liquid–solid mechanism.[8]

Altering the chemical composition of vapor species during nanowire growth and subsequent material deposition on the nanowire circumference (radial deposition) results in radial nanowire heterostructures. These radial nanowire heterostructures ultimately result in core/shell or multishell structures within a nanowire,[9] offering the flexibility to tune the band structure by using different band-gap semiconductors for core, shell, and multishell structures. Many nanowire-based devices, such as high-efficiency light-emitting diodes[9] and high-performance field-effect transistors,[10] have been demonstrated using these semiconductor heterostructures. In addition to the core/shell morphologies, islands on the nanowires are also known to form during radial deposition, through the Volmer–Weber growth mode (during FeMn radial growth on InAs nanowires)[11] and the Stranski–Krastanow growth mode (Ge radial deposition on Si nanowires).[12] This unique combination of islands and nanowires leads to the formation of hierarchical heterostructures and, in turn, may extend potential properties and consequent applications into a new technological dimension.

Herein, we report the site-selective formation of nanoscale InAs rings around GaAs nanowire cores. As shown in our earlier studies,[13] the GaAs nanowires grown in As-rich conditions show truncated triangular cross sections with {112} sidewalls. Sidewalls of the truncated edges are not planar surfaces but contain concave regions with {111} and {200} facets containing stacking faults. Heteroepitaxy on nonplanar two-dimensional surfaces is well-studied, wherein the nonplanarity influences the subsequent heteroepitaxial growth process.[14–16] It is therefore important to explore the epitaxial heterodeposition on the nonplanar sidewalls of these GaAs nanowires. To this end, we radially deposited InAs on the truncated triangular GaAs nanowires for short periods of time (two samples, with deposition durations of 1 and 5 min, respectively) and studied the radial growth process. Preferential nucleation of InAs occurred in the concave regions of the GaAs nanowire sidewalls, which subsequently led to the formation of InAs nanorings along the GaAs nanowire cores. The morphological and structural characteristics of these nanorings were determined by detailed transmission electron microscopy (TEM) investigations, from which we elucidated the formation mechanism of these nanorings.

Detailed TEM investigations also aided understanding of the radial growth behavior of InAs around GaAs nanowires. To this end, a typical InAs/GaAs nanowire with InAs grown for 1 min was imaged in different crystallographic zone axes by tilting the nanowire along its growth direction. Figure 1 a–c shows TEM images of a nanowire in $\langle 112\rangle$ and $\langle 110\rangle$ zone axes, with each zone axis tilted away from its adjacent zone axis by 30°. Careful examination of the nanowire along a $\langle 112\rangle$ zone axis (Figure 1 a) shows discontinuous presence of Moiré fringes in the center region of the nanowire along its axial direction, as marked by arrows. In comparison, no Moiré fringes can be seen when viewed along the $\langle 110\rangle$ zone axis (Figure 1 b). Instead, strain contrast can be seen on one of the nanowire sides, as marked by arrows. Careful examination on the other side of the nanowire shows Moiré fringes along the nanowire sidewall. Further tilting of the nanowire to another $\langle 112\rangle$ zone axis (Figure 1 c) exhibits the same nanowire morphology as in Figure 1 a. An electron diffraction pattern for this nanowire shows two sets of diffraction peaks, both

[*] M. Paladugu, Prof. J. Zou, Y.-N. Guo, Dr. X. Zhang
School of Engineering, The University of Queensland
Brisbane, QLD 4072 (Australia)
E-mail: j.zou@uq.edu.au
Homepage: http://www.eng.uq.edu.au/people.php?username=jinzou
H. J. Joyce, Dr. Q. Gao, Dr. H. H. Tan, Prof. C. Jagadish
Department of Electronic Materials Engineering
Research School of Physical Sciences and Engineering
The Australian National University, Canberra, ACT 0200 (Australia)
E-mail: chennupati.jagadish@anu.edu.au
Homepage: http://www.rsphysse.anu.edu.au/eme/profile.php/7
Prof. J. Zou
Centre for Microscopy and Microanalysis
The University of Queensland (Australia)
Prof. Y. Kim
Department of Physics, Dong-A University (Korea)

[**] This research is supported by the Australian Research Council. M. Paladugu acknowledges the support of an International Postgraduate Research Scholarship.

 WILEY InterScience DISCOVER SOMETHING GREAT

© 2009 Wiley-VCH Verlag GmbH & Co. KGaA, Weinheim

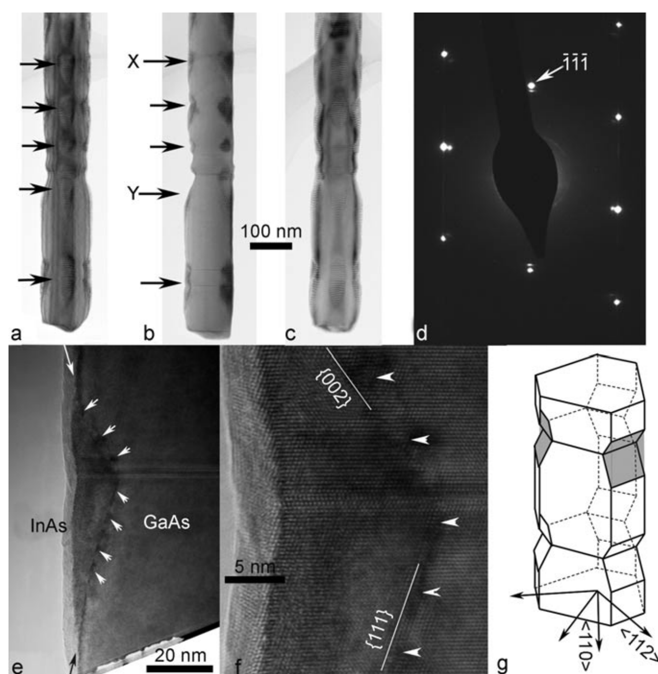

Figure 1. TEM images of InAs/GaAs nanowires after 1 min InAs growth on a) ⟨112⟩, b) ⟨110⟩, and c) another ⟨112⟩ zone axes. d) Electron diffraction pattern of an InAs/GaAs nanowire along the ⟨110⟩ zone axis. e) High-magnification TEM image and f) HRTEM image of selectively nucleated InAs in a concave region of the GaAs nanowire sidewall. g) Schematic diagram of a section of GaAs nanowire with initially nucleated InAs in the concave regions.

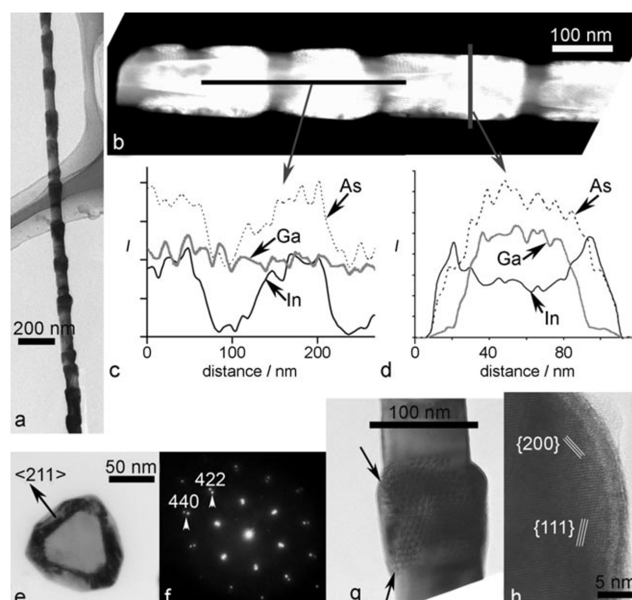

Figure 2. TEM images of InAs/GaAs nanowires after 5 min InAs growth: a) Low-magnification TEM image showing InAs nanorings along the GaAs nanowire core. b) STEM dark-field image with c, d) corresponding EDS analyses. e) TEM image of the cross section of an InAs/GaAs nanowire with f) its corresponding electron diffraction pattern. g) High-magnification TEM image of an InAs nanoring, viewed along the ⟨110⟩ zone axis, with h) its corresponding HRTEM image.

corresponding to the zinc blende structure (Figure 2 d), which typically gives rise to electron diffraction patterns along the [1$\bar{1}$0] zone axis. The lattice parameter of GaAs ($a = 0.565$ nm) is smaller than that of InAs ($a = 0.606$ nm), suggesting that the outer set of the diffraction pattern arises from GaAs and the inner set from InAs. By measuring the corresponding lattice spacings from two sets of electron diffraction patterns, a (6.5 ± 1.0) % lattice mismatch between two sets of electron diffraction patterns can be determined, which is nearly identical to their equilibrium lattice mismatch of 7.2 %. This result suggests that the discontinuous presence of Moiré fringes and the areas of strain contrast (Figure 1 a–c) must result from the relaxed InAs around the GaAs nanowires. Figure 1 e is a high-magnification TEM image of a region in Figure 1 b (marked with X), where the InAs/GaAs interface can be clearly identified. Spot-like dark contrasts (marked by arrows) can be seen, which relate to the defects between InAs and GaAs. To clarify this point, high-resolution (HR) TEM was conducted (Figure 1 f, arrows indicate misfit dislocations). It is of interest to note from that the InAs growth has selectively taken place in concave regions of the GaAs sidewalls, and no InAs can be seen between the concave regions (Figure 1 b,e). It is also evident that the concave regions of the GaAs nanowire sidewall are not filled completely with InAs (Figure 1 b, comparison of X and Y). HRTEM images (Figure 1 f) reveal that the concave regions consist of {002} and {111} facets, with a stacking fault in the middle (detailed structural characteristics can be found in Ref. [13]). A schematic diagram of a nanowire, based on these results, with a truncated triangular cross section and selectively nucleated InAs in the concave regions, is shown in Figure 1 g. The arrows correspond to the different TEM imaging directions in Figure 1 a–c.

To understand the later stages of InAs growth, we examined the InAs/GaAs nanowires after 5 min InAs growth. In the TEM image of a typical nanowire (Figure 2 a), discontinuous aggregates of InAs are visible as a discontinued strain contrast along the axial directions of the nanowire. To clarify the chemical composition of the nanowire, scanning TEM (STEM, Figure 2 b) and energy-dispersive spectroscopy (EDS, Figure 2 c, d) analyses were carried out. The results further confirmed the formation of discontinuous InAs shells, in the form of rings, around the GaAs nanowire core. To clarify the characteristics of these core–ring structures, cross section TEM specimens were characterized (Figure 2 e, f). The truncated triangular morphology of the GaAs core and its InAs shell can be distinguished through the strain contrast in the TEM image (Figure 2 e). By correlating the TEM image and the electron diffraction pattern (Figure 2 f), {112} side-facets of the truncated triangular cross sections of the nanowires can be determined. To determine any relationship between this discontinuous InAs shell formation (Figure 2) and the preferential InAs growth in the concave regions (Figure 1), we imaged the nanorings at higher magnification (Figure 2 g). As indicated by arrows, a concave region can be identified by the disappearance of the Moiré fringes, which is identical to the concave morphology shown in Figure 1 e. This contrast is found for all of the nanorings, suggesting that the preferential InAs growth in the concave regions of the GaAs

 © 2009 Wiley-VCH Verlag GmbH & Co. KGaA, Weinheim

nanowire sidewalls led to the formation of nanorings. The InAs nanoring structure is faceted on the other side of the concave region (Figure 2 g). To understand these facets, HRTEM analysis was conducted (Figure 2h), showing that these facets correspond to {200} and {111} atomic planes. These planes are often the stable facets for nanowires with {112} sidewalls.[13,17]

To understand the driving force behind the preferential growth of InAs, we examined the initial stages of InAs growth in the concave regions. Figure 3a is a high-magnification TEM image taken from the location Y in Figure 1b, showing the initially grown InAs around the edges of the concave region. Nucleated InAs can be identified by the presence of the strain contrast (indicated by the arrows). Figure 3b,c shows HRTEM images of nucleated InAs with misfit dislocations at the InAs/GaAs interface (indicated by the arrows). These misfit dislocations denote the InAs/GaAs interface. Each concave region is accompanied with stacking faults in its middle region (Figure 1 f), so that we cannot rule out the possibility that these stacking faults are favorable nucleation sites for InAs, as in the case of heterogeneous nucleation of materials at defect sites.[18] However, we found no nucleation of InAs at the stacking faults away from the concave regions, for example, at the stacking faults above the concave region in Figure 3b. This result suggests that the concave regions are essential for selective InAs growth.

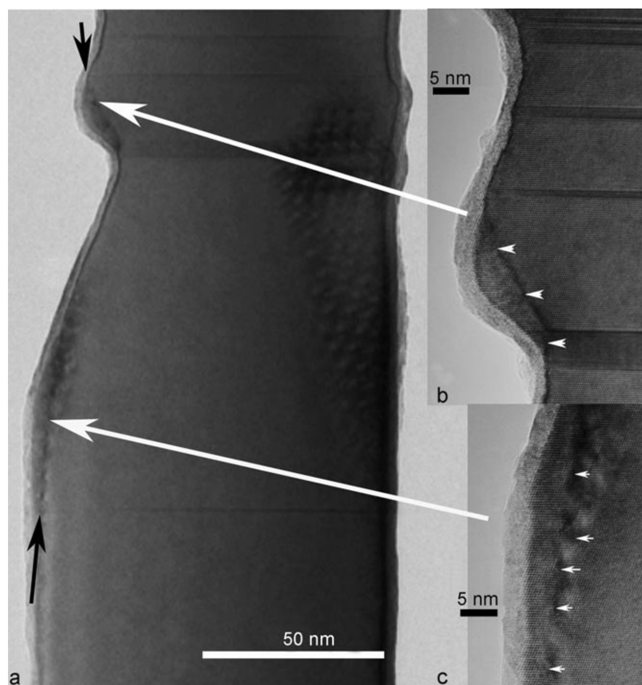

Figure 3. a) TEM image of initial growth of InAs in a concave region of the GaAs nanowire with (b, c) corresponding HRTEM images.

To understand the preferential heteroepitaxial deposition in the concave regions, we considered the surface chemical potential gradient along a nonplanar surface, which is known to be a thermodynamic driving force for epitaxy.[19–21] The chemical potential (μ) of a nonplanar surface can be expressed as in Equation (1), where μ_0 is the chemical

$$\mu = \mu_0 + \Omega\, E_s(x,y) + \Omega\, \gamma\, \kappa(x,y), \quad (1)$$

potential for a planar surface, E_s(x,y) is the local strain energy at the surface, and Ω is the atomic volume of the species. $\Omega\,\gamma\,\kappa(x,y)$ describes the surface free energy (γ) as a function of the surface curvature $\kappa(x,y)$. In the early stages of InAs deposition, when the atoms from the vapor phase make contact with the sidewalls of GaAs nanowires, the chemical potential gradient along the surfaces of sidewalls leads to the migration of these adatoms to regions of lower chemical potential, and stable nuclei form in these regions.[22,23] During the initial InAs nucleation, since InAs has a larger lattice parameter than GaAs, InAs grew preferentially at the two convex edges of the concave regions for effective strain relaxation, minimizing the misfit dislocation formation at this initial stage.[24,25] The presence of concave regions leads to the capillarity effect, as the concave regions increase the local surface free energy of GaAs, owing to the contribution of the curvature term $\kappa(x,y)$ in Equation (1). The capillarity effect reduces the chemical potential in the concave regions and leads to the diffusion of adatoms towards them.[26,27] Moreover, InAs shows lower surface energy than GaAs.[28–30] This synergistic effect drives the migration of the adatoms into the concave regions. Stable nuclei of InAs will form and grow in these regions to minimize the local surface energy. Since the capillarity effect was evident even in the absence of a lattice mismatch between the deposited material and its underlying substrate,[26] we propose that the capillarity is the key mechanism for site-selective nucleation of InAs in the concave regions.

Once these concave regions are filled, further InAs growth is driven by lowering the chemical potential which is proportional to the ratio of the surface/interface to the volume.[31] To lower the chemical potential during the further InAs growth, InAs is preferentially deposited around the concave regions, where the volume of InAs increases substantially, whereas the increase of surface and interface is marginal. As a consequence, heterogeneous InAs nanorings form by joining the three radially distributed concave regions (Figure 1 g). The nanorings formed under the current growth conditions are often isolated from each other.

From a practical point of view, these nanorings can act as quantum rings (where free electrons are confined within the rings) when they are covered with GaAs or other, higher bandgap, semiconductor materials. These structures can exhibit many potential properties, as in the case of InAs/GaAs quantum well structures. For nanorings to be useful, it is important to be able to manipulate their sizes and the distance between adjacent nanorings. Such manipulation can be achieved by varying the growth conditions, such as the duration of deposition and/or the density of twin boundaries.[32]

It is anticipated that such hierarchical nanoring/nanowire heterostructures can exhibit extraordinary physical properties, and can be used as building blocks to extend the applications of semiconductor nanostructures.

 © 2009 Wiley-VCH Verlag GmbH & Co. KGaA, Weinheim

In summary, we have demonstrated the formation of nanorings during radial deposition of InAs on GaAs nanowires. The formation mechanism of these nanorings was determined through detailed TEM studies. At the initial stages of the InAs radial deposition, InAs nucleates preferentially in the concave regions of GaAs nanowire sidewalls as a result of the capillarity effect, Further growth of InAs results in the merging of radially distributed concave regions and leads to the nanoring formation.

Experimental Section

InAs/GaAs nanowires were grown using 30 nm diameter Au nanoparticle catalysts in a horizontal-flow low-pressure (100 mbar) metal–organic chemical vapor deposition reactor, at a growth temperature of 450°C. Initially, GaAs nanowires were grown on $(\bar{1}\bar{1}\bar{1})_B$ GaAs substrates for 30 min under a flow of trimethylgallium (TMG, 1.2×10^{-5} mol min^{-1}) and AsH_3 (5.4×10^{-4} mol min^{-1}). InAs was deposited on the resultant GaAs nanowires (two samples, with deposition durations of 1 min and 5 min, respectively) by replacing the flow of TMG and with a flow of trimethylindium (TMI, 1.2×10^{-5} mol min^{-1}), while maintaining constant AsH_3 flow. The morphological and structural characteristics of the nanowires were investigated by scanning electron microscopy (SEM, JEOL 890) and transmission electron microscopy (TEM, Philips Tecnai F20 equipped with scanning transmission electron microscopy (STEM) and energy-dispersive spectroscopy (EDS) facilities). TEM specimens were prepared by ultrasonicating the nanowires in ethanol for 10 min and dispersing them on holey carbon films. Cross sections of the InAs/GaAs radial nanowire heterostructures were prepared by embedding the nanowires in resin and then by cutting them in cross section using an ultra microtome

Received: September 20, 2008
Revised: October 20, 2008
Published online: December 12, 2008

Keywords: chemical vapor deposition · electron microscopy · indium · nanostructures · surface analysis

[1] A. D. Yoffe, *Adv. Phys.* **1993**, *42*, 173.
[2] J. V. Barth, G. Costantini, K. Kern, *Nature* **2005**, *437*, 671.
[3] H. J. Fan, P. Werner, M. Zacharias, *Small* **2006**, *2*, 700.
[4] A. J. Mieszawska, R. Jalilian, G. U. Sumanasekera, F. P. Zamborini, *Small* **2007**, *3*, 722.
[5] W. Lu, C. M. Lieber, *Nat. Mater.* **2007**, *6*, 841.
[6] M. Paladugu, J. Zou, Y. N. Guo, G. J. Auchterlonie, Y. Kim, H. J. Joyce, Q. Gao, H. H. Tan, C. Jagadish, *Appl. Phys. Lett.* **2007**, *91*, 133115.
[7] M. Paladugu, J. Zou, Y. N. Guo, X. Zhang, H. J. Joyce, Q. Gao, H. H. Tan, C. Jagadish, Y. Kim, *Appl. Phys. Lett.* **2008**, *93*, 201908.
[8] R. S. Wagner, W. C. Ellis, *Appl. Phys. Lett.* **1964**, *4*, 89.
[9] F. Qian, S. Gradecak, Y. Li, C. Y. Wen, C. M. Lieber, *Nano Lett.* **2005**, *5*, 2287.
[10] J. Xiang, W. Lu, Y. J. Hu, Y. Wu, H. Yan, C. M. Lieber, *Nature* **2006**, *441*, 489.
[11] D. G. Ramlan, S. J. May, J. G. Zheng, J. E. Allen, B. W. Wessels, L. J. Lauhon, *Nano Lett.* **2006**, *6*, 50.
[12] L. Pan, K. K. Lew, J. M. Redwing, E. C. Dickey, *Nano Lett.* **2005**, *5*, 1081.
[13] J. Zou, M. Paladugu, H. Wang, G. J. Auchterlonie, Y. N. Guo, Y. Kim, Q. Gao, H. J. Joyce, H. H. Tan, C. Jagadish, *Small* **2007**, *3*, 389.
[14] S. Kohmoto, H. Nakamura, T. Ishikawa, K. Asakawa, *Appl. Phys. Lett.* **1999**, *75*, 3488.
[15] S. Jeppesen, M. S. Miller, D. Hessman, B. Kowalski, I. Maximov, L. Samuelson, *Appl. Phys. Lett.* **1996**, *68*, 2228.
[16] M. Borgstrom, J. Johansson, L. Samuelson, W. Seifert, *Appl. Phys. Lett.* **2001**, *78*, 1367.
[17] M. A. Verheijen, R. E. Algra, M. T. Borgstrom, G. Immink, E. Sourty, W. J. P. van Enckevort, E. Vlieg, E. Bakkers, *Nano Lett.* **2007**, *7*, 3051.
[18] R. D. Doherty in *Physical Metallurgy, Chapter 15: 4th revised and enhanced ed.* (Eds.: R. W. Chan, P. Haasen), North-Holland, Amsterdam, **1996**, pp. 1385–1389.
[19] D. J. Srolovitz, *Acta Metall* **1989**, *37*, 621.
[20] M. Borgstrom, V. Zela and W. Seifert, *Nanotechnology* **2003**, *14*, 264.
[21] N. Motta, P. D. Szkutnik, M. Tomellini, A. Sgarlata, M. Fanfoni, F. Patella, A. Balzarotti, *C. R. Phys.* **2006**, *7*, 1046.
[22] B. D. Gerardot, G. Subramanian, S. Minvielle, H. Lee, J. A. Johnson, W. V. Schoenfeld, D. Pine, J. S. Speck, P. M. Petroff, *J. Cryst. Growth* **2002**, *236*, 647.
[23] J. A. Venables, *Surf. Sci.* **1994**, *300*, 798.
[24] S. O. Cho, Z. M. Wang, G. J. Salamo, *Appl. Phys. Lett.* **2005**, *86*, 113106.
[25] R. D. Doherty in *Physical Metallurgy, Chapter 15: 4th revised and enhanced ed.* (Eds.: R. W. Chan, P. Haasen), North-Holland, Amsterdam, **1996**, pp. 1378–1380.
[26] G. Biasiol, A. Gustafsson, K. Leifer, E. Kapon, *Phys. Rev. B* **2002**, *65*, 205306.
[27] J. G. Biasiol, E. Kapon, *Phys. Rev. Lett.* **1998**, *81*, 2962.
[28] L. G. Wang, P. Kratzer, M. Scheffler, *Jpn. J. Appl. Phys. Part 1* **2000**, *39*, 4298.
[29] E. Pehlke, N. Moll, A. Kley, M. Scheffler, *Appl. Phys. A* **1997**, *65*, 525.
[30] N. Moll, A. Kley, E. Pehlke, M. Scheffler, *Phys. Rev. B* **1996**, *54*, 8844.
[31] M. Zinkeallmang, L. C. Feldman and M. H. Grabow, *Surf. Sci. Rep.* **1992**, *16*, 377.
[32] H. J. Joyce, Q. Gao, H. H. Tan, C. Jagadish, Y. Kim, X. Zhang, Y. N. Guo, J. Zou, *Nano Lett.* **2007**, *7*, 921.

© 2009 Wiley-VCH Verlag GmbH & Co. KGaA, Weinheim